Journal of Rehabilitation in Civil Engineering 1-1 (2013) 66-77

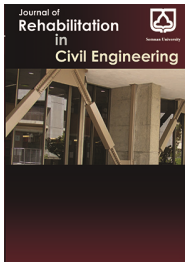

journal homepage: http://civiljournal.semnan.ac.ir/

Flexural Behavior of Reinforced HPFRCC Beams

A. Hemmati[1*], A. Kheyroddin[2] and M. K. Sharbatdar[3]

1. Ph.D. Student, Civil Engineering Faculty, Semnan University, Semnan, Iran.
2. Professor, Civil Engineering Faculty, Semnan University, Semnan, Iran.
3. Associate Professor, Civil Engineering Faculty, Semnan University, Semnan, Iran.
Corresponding author: *ahemmati2000@yahoo.com*

ARTICLE INFO

Article history:
Received: 5 October 2012
Accepted: 9 January 2013

Keywords:
Finite Element
Plastic Hinge
Reinforced Concrete
Rotation Capacity

ABSTRACT

High Performance Fiber Reinforced Cementitious Composite (HPFRCC) materials exhibit strain hardening behavior with multiple cracking under tensile loading. In this paper, experimental and parametric studies are performed to assess the influence of using HPFRCC material instead of normal concrete in reinforced concrete beams. After calibrating the experimental results, the analytical results including ductility and plastic hinge characteristics for simply supported beams with different values of compressive strengths are presented and compared with each other and also with the experimental data, where available. The analytical and experimental results indicate that using HPFRCC material instead of normal concrete in RC beams concluded to an increase in ultimate load, deflection, ductility ratio, plastic hinge length and rotation capacity compared to RC beams. In RH beam, fibers act as extra steel reinforcements and high ductility of this beam is attained by existence of this fibers and bridging mechanism of them which prevent the crushing of compressive HPFRCC material.

1. Introduction

HPFRCC (High Performance Fiber Reinforced Cementitious Composite) is a material with strain hardening response under uni-axial loading. At the first stages, Li and Wu introduced a pseudo-strain-hardening material with fine aggregates and reinforcing polyethylene fibers [1]. In 1996, Naaman and Reinhardt developed a fiber reinforced cementitious material which had a matrix with no coarse aggregates, and was regarded as fiber reinforced cement paste or mortar [2]. High tensile ductility with strain hardening response was the most important characteristic of this material [3-4]. A great amount of researches which have been performed in recent years, focused on the

durability and steel corrosion of partially layered RC beams with HPFRCC material [5-6]. Moreover, some numerical works have been performed by Kabele for numerically simulating of an HPFRCC overlay cast on an un-reinforced concrete beam with a notched fracture [7-8].

In this paper, an experimental work was carried out and then a nonlinear finite element program was used for performing a parametric study to examine the influence of compressive strength of HPFRCC and concrete and steel reinforcement ratios on ultimate deformation and plastic hinge characteristics of RC beams.

2. Experimental program

The test specimens which were chosen for this study were two large scale beams with two hinged supports which have been tested by authors. Details of reinforcement layout and loading of the beams are shown in Fig. 1. Strain gauges were installed according to Fig. 2 in some positions of both reinforced concrete (RC) and reinforced HPFRCC (RH) beams.

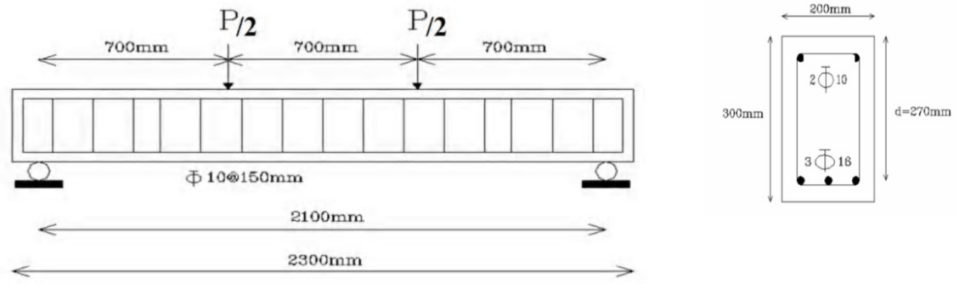

Fig. 1. Details of the experimental specimens

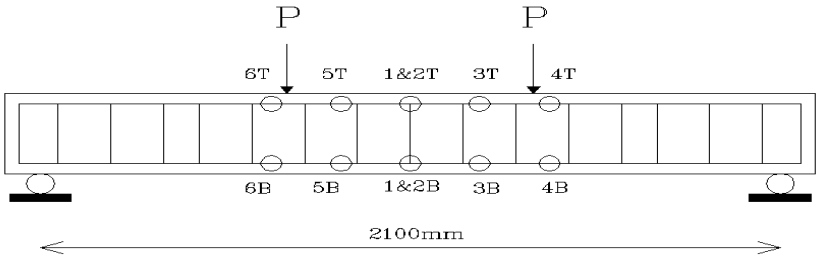

Fig. 2. Location of installed strain gauges

Mix proportions of the concrete and HPFRCC materials are presented in Table 1. The mixture ratios were based on the weight of cement. Coarse aggregate was not used in HPFRCC material, but Polypropylene (PP) fibers with a length of 12 mm and diameter of 18 μm used for achieving the HPFRCC. Coarse aggregate gradations taking 4.75 to 12.5 mm particles and fine aggregate gradations taking particles less than 4.75 mm were used too. During the mixing, care was taken to prevent clumping of the fibers. The dry components of the mortar mix were first combined with approximately 25% of the total water required and then the fibers along with the remaining 75% of the water were intermittently added as the mixing process progressed. The fibers were added slowly, while mixing continued in order to distribute the fibers thoroughly throughout the mix. To

determine the compressive properties of the concrete and HPFRCC material, compression test on 100 x 100 mm cubes specimens was performed as shown in Fig. 3-a and compressive failure of these specimens are presented in Fig. 3-b. As shown in this figure, due to presence of PP fibers, the HPFRCC maintained its integrity under loading and consequently showed ductile behavior. Material properties are shown in Table 2. Test set up of reinforced concrete (RC) and reinforced HPFRCC (RH) beams is presented in Fig. 4.

Table 1. Mix proportion of concrete and HPFRCC

Material	Cement	Coarse Aggregate	Fine Aggregate	Water	Fiber
Concrete	1	1.72	1.72	0.48	-
HPFRCC	1	-	1	0.54	1 %(Volume Fraction)

(a) (b)

Fig. 3. Compression test of concrete and HPFRCC specimens

Table 2. Concrete, HPFRCC and steel properties used in the test beams

Material properties	(RC beam)	(HPFRCC beam)
$f_c'\ (MPa)$	24	24
$f_y\ (MPa)$	400	400
$E_s\ (MPa)$	200,000	200,000

Fig. 4. Test Set-up

The vertical load was applied on RC beam and the first cracking observed at the load of 46 kN and mid-span deflection of 1.29 mm respectively at the mid-span of the beam as shown in Fig. 5. Then the yielding of steel bars occurred at the load of 126.4 kN and deflection of 6.57 mm. Further loading caused the cracking spread at the bottom face of the beam as shown in Fig. 6. Finally beam carried the load of 238.08 kN and deflection of 34.47 mm. Condition of the RC beam at the ultimate load and displacement is shown in Fig. 7. As shown in these figures, the failure was in flexural mode, i.e. at first step

tensile reinforcements started to yield and then compressive crushing of concrete occurred. The failure was accompanied by large tensile cracks in lower parts of the section in mid-span of the beam. The amount of damage in compressive concrete was severed and ultimate deflection was small.

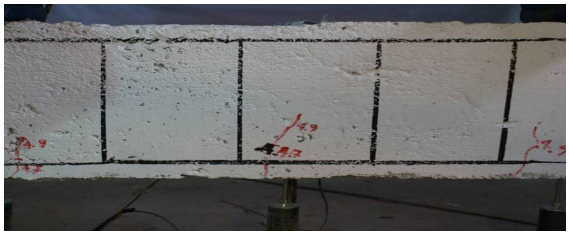

Fig. 5. Initial cracks in RC beam

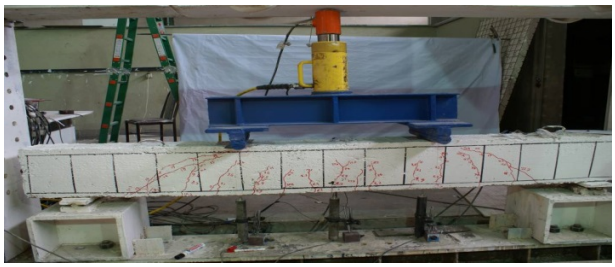

Fig. 6. Spread of cracking in RC beam

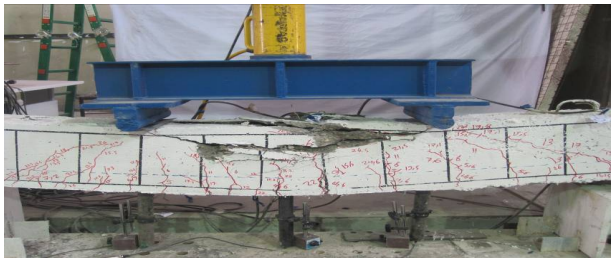

Fig. 7. RC beam at the end of test loading

In the case of RH beam, the first cracking observed at the load of 45 kN and mid-span deflection of 1.46 mm respectively at the mid-span of the beam and then the yielding of steel bars occurred at the load of 138.24 kN and deflection of 6.66 mm. Finally beam carried the load of 253.44 kN and deflection of 60.45 mm. Condition of the RH beam at the ultimate load and displacement is shown in Fig. 8.

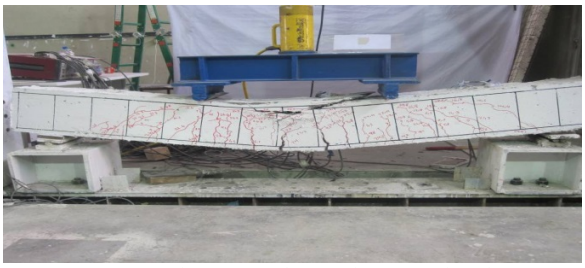

Fig. 8. RH beam at the end of test loading

Load-deflection curves of these two test specimens are presented in Fig. 9. Summary of these experimental results and strain values in some point of the beams are presented in Tables 3 and 4. Where, $\mu = \frac{\Delta_u}{\Delta_y}$.

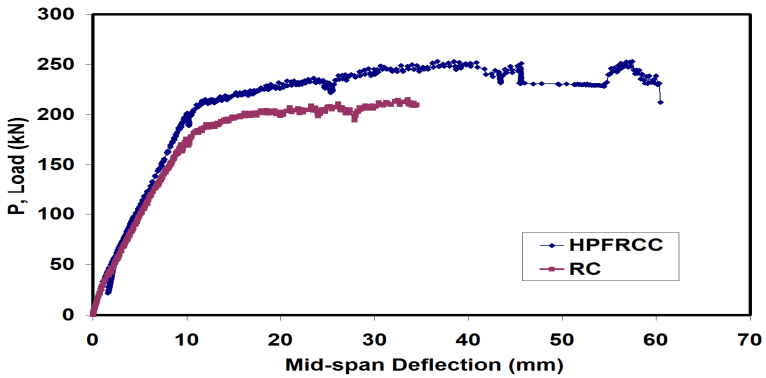

Fig. 9. Load-deflection curves of experimental specimens

Table 3. Summary of experimental results

Specimen	P_y (kN)	P_u (kN)	Δ_y (mm)	Δ_u (mm)	μ	$\frac{\mu}{\mu_{RC}}$
RC	126.4	238.08	6.57	34.47	5.25	1
RH	138.24	253.44	6.66	60.45	9.08	1.73

Table 4. Strain values in RC and RH specimens at yielding point

No.	RC	RH
1B	1700.23	1547.85
2B	1622.2	1739.63
3B	1447	1780.91
4B	1631.46	1894
5B	1785	1584
6B	2125	2057

3. Nonlinear finite element program and calibration

Some researchers have been developed plasticity based models for HPFRCC material [7, 9, 10]. But, there are some computer programs for modeling of concrete and cement composites. The experimental beams which were tested in this paper, also analyzed using the available nonlinear finite element software called ABAQUS. In a nonlinear analysis, ABAQUS automatically chooses appropriate load increments and convergence tolerances and continually adjusts them during the analysis to ensure that an accurate solution is obtained efficiently [11]. The envelope curves of concrete and HPFRCC were entered in this software and then analytical models calibrated with experimental works [12]. Monotonic tension and compression, and cyclic testing of HPFRCC material which were developed by some researchers [13] concluded to a constitutive model for HPFRCC for simulating the behavior of this material [14]. The loading and unloading parts for this proposed constitutive model are shown in Fig. 10.

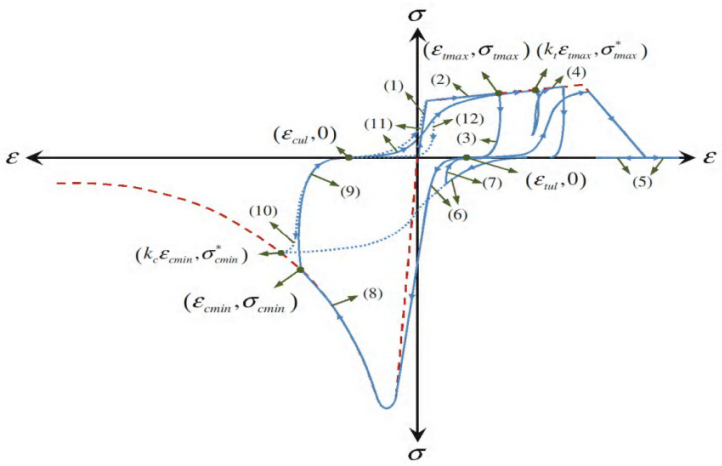

Fig. 10. HPFRCC constitutive model [14]

This proposed constitutive model includes four segments which were numbered in Fig. 10. Envelope curves (segments 1, 2, 5 and 8), unloading curves (segments 3 and 9), reloading curves (segments 4 and 10) and transition from tension to compression (segments 6, 7, 11 and 12) are four parts of discussed constitutive model. Where, E= Modulus of Young, ε_{t0}= First cracking strain, σ_{t0}= First cracking stress, ε_{tp}= Strain at peak stress in tension, σ_{tp}= Strength in tension, ε_{tu}= Tensile strain capacity, ε_{cp}= Strain at peak stress in compression, σ_{cp}= Strength in compression, ε_{cu}= Ultimate strain in compression and σ_{cr}= Stress corresponding to ε_{cu}.

An envelope curve is attained by joining the maximum points of stress at every strain value in the loading history. Monotonic tests conducted on HPFRCC material indicate that the tensile behavior is characterized by three distinct parts including linear elastic behavior until ε_{t0}, strain hardening behavior associated with multiple cracking until ε_{tp} and softening behavior after this point as shown in Fig. 11-a. The shape of compression envelope for post-peak response is similar to that observed in concrete. However, the prepeak response of the ECC is observed to be better represented by a linear elastic relationship up to 2/3 of the strain corresponding to peak stress as shown in Fig. 11-b. For higher strain values the equation proposed by Saenz (Saenz 1964), and shown in Fig. 11-b, is used to simulate the compression envelope for the ECC constitutive model [14].

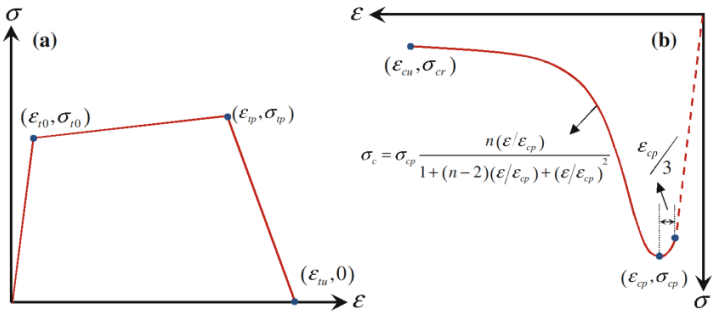

Fig. 11. Tension and compression envelope curves of HPFRCC [14]

In this paper, two groups of beams including RC and RH beams are analyzed using ABAQUS program. To investigate the influence of mesh size on the nonlinear analysis results, three types of mesh configurations were used for analyzing these beams. These mesh configurations including coarse, medium and fine mesh sizes. Load-mid span deflection curves for these RC and RH beams are shown in Fig. 12 and Fig. 13.

In RC beam, the medium mesh size (50mm x 50mm), gave an ultimate load value of 236.46 kN, which was close to the experimental value 238.08 kN. While the coarse mesh size (100mm x 100mm), results in an ultimate load value 289.17 kN and the fine mesh size (25mm x 25mm), concludes to an ultimate load 180.44 kN. Both of these values are far from the experimental value. These analytical results are summarized in Table 5.

In RH beam, the medium mesh size (50mm x 50mm) gave an ultimate load value of 259.5 kN, which was close to the experimental value 253.44 kN. These analytical results are summarized in Table 6.

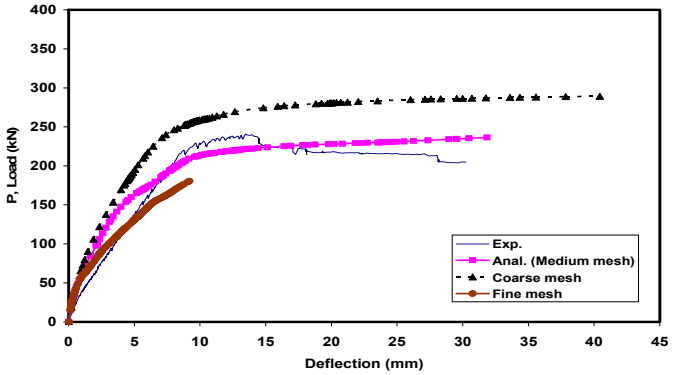

Fig. 12. Load-mid span deflection curves for different mesh sizes in RC beam

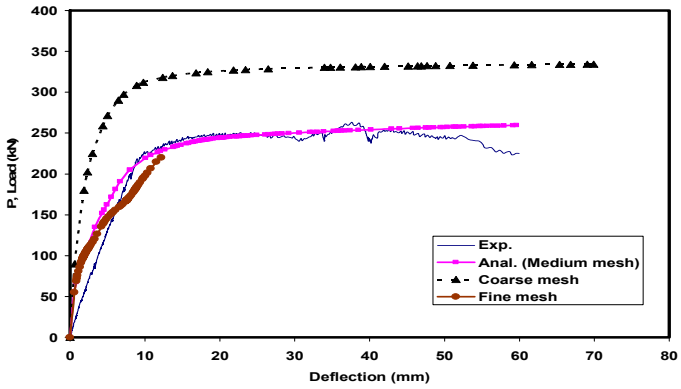

Fig. 13. Load-mid span deflection curves for different mesh sizes in RH beam

Table 5. Analytical and experimental results for RC beams with different mesh sizes

Size of elements (mm x mm)	P_u (kN)	Δ_u (mm)	$\frac{P_u(Analytical)}{P_u(Experimental)}$	M_u (kN.m)
Experimental	238.08	34.47	-	83.33
25 x 25	180.44	9.18	0.76	63.15
50 x 50	236.46	31.84	0.99	82.76
100 x 100	289.17	40.43	1.21	101.21

Table 6. Analytical and experimental results for RH beams with different mesh sizes

Size of elements (mm × mm)	P_u (kN)	Δ_u (mm)	$\frac{P_u(Analytical)}{P_u(Experimental)}$	M_u (kN.m)
Experimental	253.44	60.45	-	88.7
25 x 25	220	12.18	0.87	77
50 x 50	259.5	59.61	1.02	90.83
100 x 100	334.26	69.93	1.32	116.99

Cracking was idealized using the smeared cracking model, and assumed to occur when the principal tensile stress at a point (usually a Gauss integration point) exceeded the concrete tensile strength. The stiffness across the crack is assumed to be zero and the principal directions are not allowed to rotate.

4. Results and Discussion

Load deflection curves of RC models with different compressive strengths including 24, 35 and 39 MPa are illustrated in Fig. 14. Load deflection curves of corresponding RH models are illustrated in Fig. 15. The

analytical results including the ultimate loads and ductility ratios of these analytical beams are also presented in Table 7. The mode of failure is flexural for all beams. As shown in these figures and tables, ultimate load, deflection and ductility ratio of RC-39 beam are about 2.74 %, 6.5 % and 11 % higher than its corresponding values in RC-24 beam. In RH-39 beam, the ultimate load, deflection and ductility ratio are about 2.36 %, 3.27 % and 11 % more than that of RH-24 respectively. Load and deflection capacity and ductility ratio of reinforced concrete and HPFRCC beams increase with increasing the compressive strength of concrete and HPFRCC. Load and deflection capacities and ductility ratios of RH models are about 10.5 %, 90.7 % and 1.78 times more than corresponding values in RC models. This may be due to existence of reinforcing fibers and HPFRCC material maintains its integrity under severe loading (bridging mechanism and pull out of fibers) and subsequently steel reinforcements suffer more strains and reach more close to the value of their plastic strain. Moreover, the ultimate compressive strain of HPFRCC is more than normal concrete.

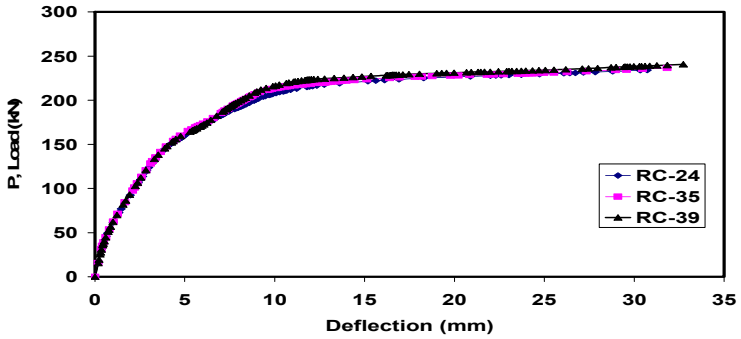

Fig. 14. Load deflection curves of RC models with different compressive strengths

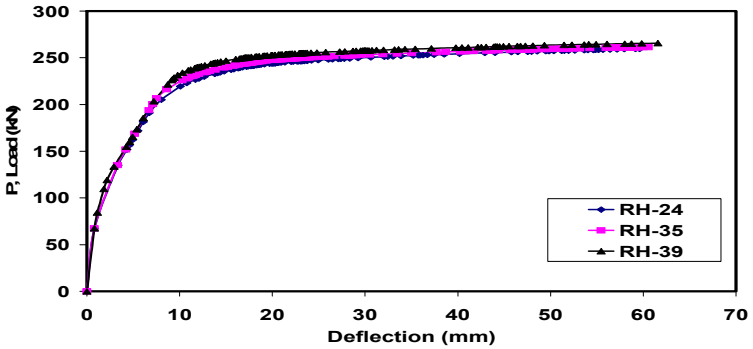

Fig. 15. Load deflection curves of RH-3.5-24, RH-3.5-35 and RH-3.5-39

Table 7. Analytical results for RC and RH beams with different compressive strengths

Model name	Δ_y (mm)	P_u (kN)	Δ_u (mm)	$\mu_\Delta = \frac{\Delta_u}{\Delta_y}$	$\frac{\mu}{\mu_{RC}}$
RC-24	6.37	234.12	30.73	4.82	1
RC-35	6.16	236.46	31.84	5.17	1.07
RC-39	6.11	240.54	32.73	5.36	1.11
RH-24	6.87	259.5	59.61	8.68	1.8
RH-35	6.63	261.49	60.55	9.13	1.89
RH-39	6.4	265.63	61.56	9.62	1.99

For calculating the of θ_p and l_p values, the curvature along the beam is obtained from the concrete and HPFRCC strain values in compression zone and from the steel strain in tension zone at the ultimate limit state. Then the θ_p is calculated by integration along the yielding length. Curvature distributions in RH-24 and RC-24 beams along their yielding length are presented in Fig. 16. Plastic hinge characteristics including the yielding length (l_y), plastic hinge length (l_p) and plastic hinge rotation (θ_p) of these beams are also presented in Table 8. It is obvious that these parameters in RH beams are higher than corresponding values in RC beams. As it shown in Table 8, plastic hinge length and rotation of RH beams are about 1.065 and 1.77 times more than that of that of RC beams. But the yield length in both beams is the same approximately. This may be due to existence of reinforcing fibers, HPFRCC material maintains its integrity under severe loading and subsequently steel reinforcements suffer more strains and get closer to the value of their plastic strain. Moreover, the ultimate compressive strain of HPFRCC is more than normal concrete. This phenomenon concludes to increase in ultimate curvature, plastic hinge length and plastic hinge rotation of RH beams compared to RC beams.

Load deflection curves of RH beams with different tensile reinforcement ratios (ρ) are illustrated in Fig. 17. The analytical results including the ultimate loads, deflections, curvatures and ductility ratios for these beams are also presented in Table 9. The mode of failure is flexural for all of these beams. As shown in Fig. 17 and Table 9, increasing in the value of tension reinforcement ratio in these beams conclude to higher ultimate load values. In the other hand, increasing in the value of tension reinforcement ratio of these beams conclude to less ultimate deflection, curvature and ductility ratio.

Distributions of curvatures along the yielding lengths in these analytical models are presented in Fig. 18. Plastic hinge characteristics of these beams are also presented in Table 10. It seems that increasing in the value of tension reinforcement ratio of these beams conclude to less plastic hinge length and plastic hinge rotation. The plastic hinge length of RH5, RH6, RH7 and RH8 are about 1.028, 1.01, 0.996 and 0.883 times the value obtained for RH1 beam. The plastic hinge rotation of RH5, RH6, RH7 and RH8 are about 1.386, 1.224, 0.919 and 0.619 times to the value obtained for RH1 beam.

Table 8. Plastic hinge characteristics of RC and RH beams

Model name	$\phi_u \times 10^{-6}$ (rad/mm)	l_y (mm)	l_p (mm)	θ_p (rad)	$\frac{l_p}{(l_p)_{RC}}$	$\frac{\theta_p}{(\theta_p)_{RC}}$
RC-24	54.5	550	273	0.0127	1	1
RH-24	87.4	550	290	0.0223	1.062	1.756

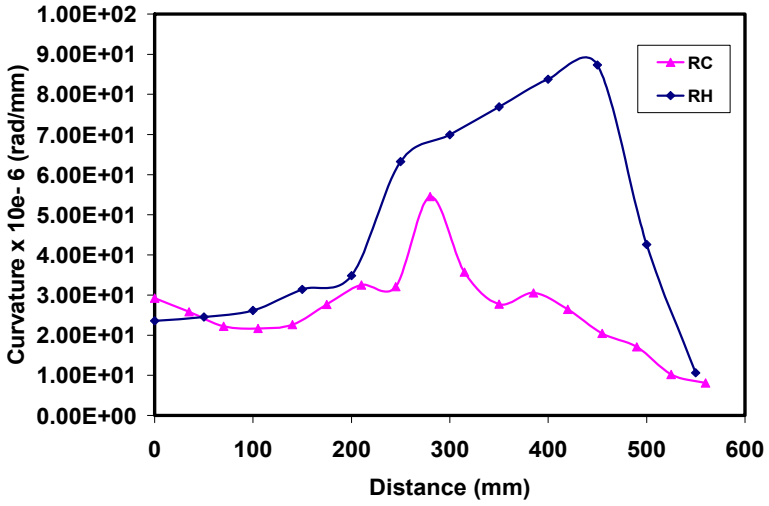

Fig. 16. Distribution of curvature in RC and RH beams

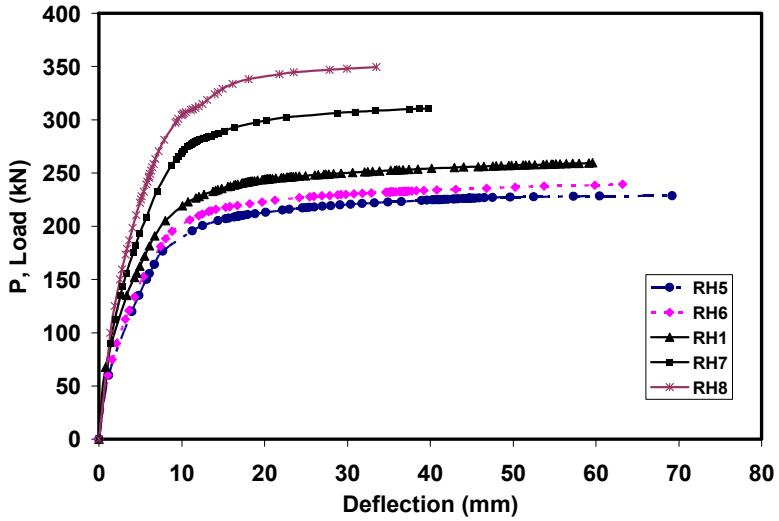

Fig. 17. Load-deflection curves of RH beams with different tensile reinforcement ratios

Table 9. Analytical results for RH beams with different tensile reinforcement ratios

Model name	ρ	Δ_y (mm)	P_u (kN)	Δ_u (mm)	$\phi_u \times 10^{-6}$ (rad/mm)	$\mu_\Delta = \frac{\Delta_u}{\Delta_y}$	$\frac{\mu}{\mu_{RC}}$
RH1	0.0112	6.87	259.5	59.61	87.4	8.67	1.78
RH5	0.006	4.71	228.62	69.21	114	14.69	3.05
RH6	0.0074	5.24	239.61	63.21	104	12.06	2.5
RH7	0.0147	9.15	310.66	39.72	79.8	4.34	0.9
RH8	0.022	13.14	349.48	33.51	63.5	2.55	0.53

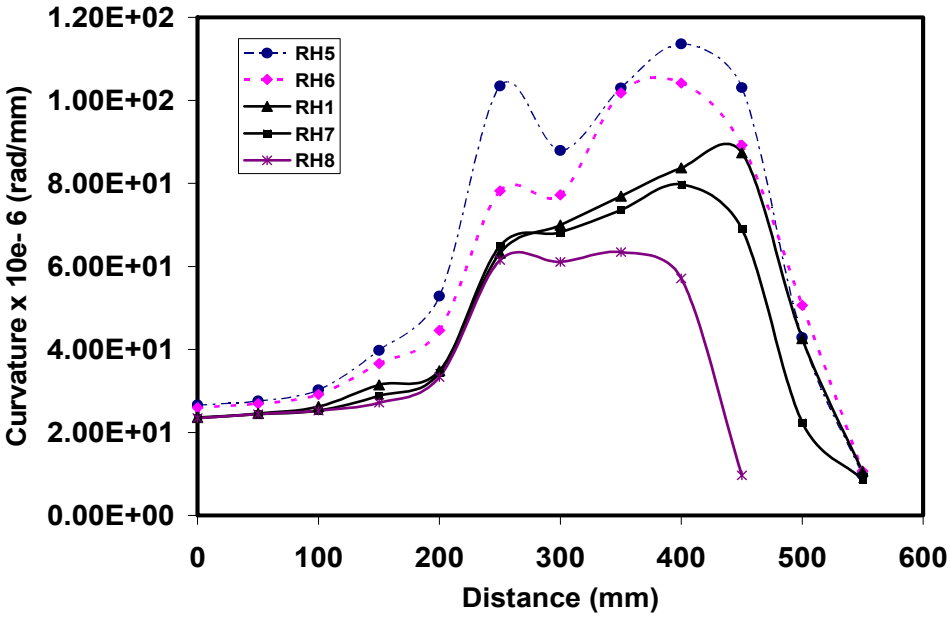

Fig. 18. Distribution of curvature in RH beams with different tensile reinforcement ratios

Table 10. Plastic hinge characteristics of RH beams with different ρ

Model name	l_y (mm)	l_p (mm)	θ_p (rad)	$\frac{l_p}{(l_p)_{RC}}$	$\frac{\theta_p}{(\theta_p)_{RC}}$
RH1	550	290	0.0223	1.062	1.756
RH5	550	298	0.0309	1.091	2.433
RH6	550	293	0.0273	1.073	2.149
RH7	550	289	0.0205	1.058	1.614
RH8	450	256	0.0138	0.938	1.086

5. Conclusions

Based on the analytical and experimental results, the following conclusions can be drawn:

1. The ultimate loads, mid-span deflections and ductility ratios of the models increase with increasing the value of compressive strength of concrete and HPFRCC.

2. The amount of damage is severe in RC models compared to RH models.

3. The yield and ultimate loads increase with increasing the tension reinforcement ratio in RH beams, but the ultimate deflection, ultimate curvature and ductility ratio decrease.

4. The value of plastic hinge length and plastic hinge rotation of RH simply

supported beams are 1.065 and 1.77 times higher than that of RC beams.

5. By substituting the normal concrete by HPFRCC material in RH beam, fibers act as extra steel reinforcements and high ductility of this beam was attained by existence of this fibers and bridging mechanism of them which prevent the crushing of compressive HPFRCC material. This mechanism had the most important role on behavior of RH beam and this improving effect concludes to more ductility ratios.

REFERENCES

[1] Li, V.C., Wu, H.C. (1992). "Conditions for pseudo strain-hardening in fiber reinforced brittle matrix composites". J. Applied Mechanics Review, Vol. 45, pp. 390-398.

[2] Naaman, A.E., Reinhardt, H.W. (1996). "Characterization of high performance fiber reinforced cement composites". HPFRCC-2, pp. 1-24.

[3] Fantilli, A.P., Mihashi, H., Vallini, P. (2007). "Crack profile in RC, R/FRCC and R/HPFRCC members in tension". Materials and Structures, Vol. 40, No. 10, pp. 1099-1114.

[4] Naaman, A.E., Reinhardt, H.W. (2006). "Proposed classification of HPFRC composites based on their tensile response". Materials and Structures, Vol. 39, No. 5, pp. 547-555.

[5] Maalej, M., Li, V.C. (1995). "Introduction of strain hardening engineered cementitious composites in design of reinforced concrete flexural members for improved durability". ACI Structural Journal, Vol. 92, No. 2.

[6] Maalej, M., Ahmed, S.F.U., Paramasivam, P. (2002). "Corrosion durability and structural response of functionally-graded concrete beams". JCI International workshop on ductile fiber reinforced Cementitious composites (DFRCC), Application and Evaluation, Japan, pp. 161-170.

[7] Kabele, P., Horii, H. (1996). "Analytical model for fracture behaviors of pseudo strain-hardening cementitious composites". Journal of Materials, Concrete Structures and Pavements, Vol. 30, pp. 208-219.

[8] Kabele, P. (2000). "Assessment of structural performance of engineered cementitious composites by computer simulation". Habilitation Thesis, Csech Technical University in Prague, pp. 46- 50.

[9] Sirijaroonchai, K. (2009). "A macro-scale plasticity model for high performance fiber reinforced cement composites". PhD Dissertation, Michigan University.

[10] Gencturk, B., Elnashai, A.S. (2009). "Analytical modeling of engineered cementitious composite members". The Asian-Pacific Network of Centers for Earthquake Engineering Research (ANCER) Workshop, University of Illinois.

[11] ABAQUS Manual. (2008). "Getting started with ABAQUS".

[12] Li, J., Zhang, Y.X. (2011). "Evolution and calibration of a numerical model for modeling of hybrid-fiber ECC panels under high-velocity impact". Composite Structures, Vol. 93, pp. 2714-2722.

[13] Kesner, K.E., Billington, S.L. (2004). "Tension, compression and cyclic testing of engineered cementitious composite materials". Technical report MCEER-04-0002.

[14] Gencturk, B., Elnashai, A.S. (2012). "Numerical modeling and analysis of ECC structures". Materials and Structures, pp. 1-20.